Frictional Properties of Feldspar-chlorite Altered Gouges and Implications for Fault Reactivation in Hydrothermal Systems

Zijuan Hu[1,2], Chongyuan Zhang[2,3,4], Lei Zhang[5], Derek Elsworth[6,7], Quan Gan[8], Huiru Lei[5], Manchao He[3], Leihua Yao[1]

[1]School of Engineering and Technology, China University of Geosciences (Beijing), Beijing 100083, China

[2]Institute of Geomechanics, Chinese Academy of Geological Sciences, Beijing 100081, China

[3]School of Mechanics and Civil Engineering, China University of Mining and Technology, Beijing 100083, China

[4]Technology Innovation Center for In-situ Stress, Ministry of Natural Resources, Beijing 100081, China

[5]State Key Laboratory of Earthquake Dynamics, Institute of Geology, China Earthquake Administration, Beijing, China

[6]Department of Energy and Mineral Engineering, EMS Energy Institute and G3 Center, the Pennsylvania State University, PA, 16802, USA

[7]Department of Geosciences, the Pennsylvania State University, University Park, PA, 16802, USA

[8]School of Resources and Safety Engineering, Chongqing University, Chongqing 400044, China

Corresponding author: Chongyuan Zhang (zhchongyuan@126.com, zhangchy@cags.ac.cn)

Key Points:

- Pure-feldspar gouges change from v-strengthening to v-weakening with elevated temperature and remain v-weakening at pore pressures
- Conversely, feldspar-chlorite altered have reduced strength but change response from v-weakening to v-strengthening
- Frictionally-unstable slip is likely on feldspar gouges but less-likely where chlorite altered, under P-T conditions of representative of deep geothermal reservoirs

Abstract

As a particularly common minerals in granites, the presence of feldspar and altered feldspar-chlorite gouges at hydrothermal conditions have important implications in fault strength and reactivation. We present laboratory observations of frictional strength and stability of feldspar (K-feldspar and albite) and altered feldspar-chlorite gouges under conditions representative of deep geothermal reservoirs to evaluate the impact on fault stability. Velocity- stepping experiments are performed at a confining stress of 95 MPa, pore pressures of 35-90 MPa and temperatures of 120-400°C representative of in situ conditions for such reservoirs. Our experiment results show that the feldspar gouge is frictionally strong (μ~0.71) at all experimental temperatures (~120-400°C) but transits from velocity-strengthening to velocity-weakening at T>120°C. Increasing the pore pressure increases the friction coefficient (~0.70-0.87) and the gouge remains velocity weakening, but this weakening decreases as pore pressures increase. The presence of alteration-sourced chlorite leads to a transition from velocity weakening to velocity strengthening in the mixed gouge at experimental temperatures and pore pressures. As a ubiquitous mineral in reservoir rocks, feldspar is shown to potentially contribute to unstable sliding over ranges in temperature and pressure typical in deep hydrothermal reservoirs. These findings emphasize that feldspar minerals may increase the potential for injection-induced seismicity on pre-existing faults if devoid of chlorite alteration.

Plain Language Summary

Granites are an important habitat for deep geothermal reservoirs where the advantages of low-carbon energy are offset by the potential hazard of injection-triggered seismicity. Feldspars in these granites are highly susceptible to water–rock interactions and produce chlorite under appropriate hydrothermal conditions. Many studies have shown that chlorite itself, as well as its coexistence with other minerals (not yet including feldspar), can generate earthquakes during fluid-injection into such reservoirs. We conduct laboratory measurements of frictional properties of simulated feldspar and chlorite gouges to determine the likelihood of spawning earthquakes. We show that high temperatures and pore pressures favor unstable slide on feldspar gouges – and thus the potential to generate earthquakes. However, chlorite as an alteration product stabilizes faults and reduces the potential for earthquakes. Our results highlight the importance of feldspar and its alteration in controlling fault strength and the potential for triggered earthquakes in geothermal reservoirs.

1 Introduction

Fluid injection triggering fault reactivation and thus induced seismicity during unconventional resource extraction such as for shale gas recovery and geothermal energy has received widespread attention (Majer et al., 2007; Ellsworth et al., 2013; Schultz et al., 2020). Large volume and high-rate injections may elevate fluid pressures and reactivate pre-existing fractures and faults and enhance the potential for induced seismicity (Hubbert & Rubey, 1959; Bao & Eaton., 2016; Faulkner et al., 2018; Schultz et al., 2020; Eyre et al., 2019). Thus, understanding mechanisms of injection-induced earthquakes is vital to mitigate the hazard (Hunfeld et al., 2017). Mature faults are typically gouge filled and thus slip nucleates on this weak component. The mineralogy of fault gouge exerts a significant control on the frictional properties (including both strength and sliding stability) and thus on the potential for induced earthquakes (Scholz, 1998, 2019; Niemeijer & Spiers, 2007; Ikari et al., 2011). Therefore, frictional properties of fault gouge, primarily the frictional strength, strength evolution with slip velocity and history (velocity and state dependence) are of great significance in defining the seismic behavior of faults. Variation in reservoir temperature as well as fluid pressures impact frictional properties and are important to define (van der Elst et al., 2013; Faulkner et al., 2018; Andrés et al., 2019; An et al., 2020).

Many previous experimental studies have explored the frictional stability of faults using both simulated and natural fault gouges spanning broad ranges of temperature and pressure, including for granites. A common feature of granite gouges is that frictional properties are strongly influenced by temperature - increasing temperature results in a transition from velocity weakening to velocity strengthening (Lockner et al., 1986; Blanpied et al., 1991, 1995). Specifically, the frictional properties of quartz and feldspar, the main constituent minerals in granites, have also been the subject of extensive experimental studies. Quartz-rich fault gouge commonly exhibits high frictional strength (μ~0.7) and promotes velocity strengthening behavior (Chester & Higgs, 1992; Tembe et al., 2010; Lu & He, 2018; Masuda et al., 2019; Bedford et al., 2022). The major feldspar-group minerals in the crust are albite ($NaAlSi_3O_8$), anorthite ($CaAl_2Si_2O_8$) and K-feldspar ($KAlSi_3O_8$). Among them, the anorthite- albite series (plagioclase) are the most abundant minerals and may modulate the response of quartz in granites. To date, few experiments define the frictional properties of feldspar under hydrothermal conditions typical of the shallow crust – representative of triggering in the recovery of deep geothermal energy. A few experimental studies define the frictional strength of plagioclase as similar to quartz, with a coefficient of friction of ~ 0.7 (Masuda, 2019, 2020). However, compared with quartz, plagioclase exhibits different frictional stability response. Over the temperature range200-500°C, plagioclase is velocity weakening with negative ($a-b$) values (Masuda, 2019, 2020; He et al., 2013) suggesting the potential for seismic reactivation.

In addition to the comminution products from granites, as quartz and feldspar, metamorphic transformations under long-term hydrothermal conditions produce important alteration products – again with potentially key controls on frictional stability (Brown et al., 2003; Okamoto et al., 2019). For example, chlorite is a widespread product of hydrothermal alteration within subducting oceanic crust and geothermal reservoirs (Elders et al., 1979; Schiffman & Fridleifsson, 1991; Morrow et al., 2000; Okamoto et al., 2019), resulting from the alteration of micas or as products of water–rock interactions (Lucie, 2016; Yuguchi et al., 2015, 2021). Chlorite is produced by the dissolution of K-feldspar in the presence of weakly alkaline pore fluids in the temperature range of 210–350 °C (Yuguchi et al., 2021), representative of deep geothermal reservoirs. Previous laboratory studies of simulated chlorite-rich gouges sheared at elevated temperatures and pore pressures indicate relatively low shear strengths (frictional coefficient μ < 0.5) although velocity strengthening behavior (Shimamoto & Logan, 1981; Ikari et al., 2009; Okamoto et al., 2019; Fagereng & Ikari, 2020; An et al., 2021). Of particular concern is that the alteration pathway from feldspar to chlorite is rapid, with the potential to evolve over engineering timescales and in fracture systems newly accessed in geothermal reservoirs. Therefore, a careful understanding of the frictional properties of pervasive feldspar chloritization is necessary in assessing and mitigating potential injection-induced seismic risks.

Typical geological hosts for deep geothermal reservoirs are granitic and with abundant low-grade metamorphic minerals (such as chlorite and epidote) developed with in the reservoirs (Okamoto et al., 2019; An et al., 2021). In addition, typical enhanced geothermal systems (EGS) reservoirs often host pyrite, indicative as a geothermometer of hydrothermal intrusion > 250°C (Zhang et al., 2022) - with 250 °C present within the stability field for chlorite. In addition, K-feldspar is hydrolyzed in a weakly alkaline environment at this temperature and with the potential to form chlorite. Such strong feldspar-chlorite alteration is apparent in the Matouying EGS reservoir of North China (Figure 1). To constrain the impact of such alteration pathways on the stability of faults in such generic granitic reservoirs, we conduct friction-stability experiments on feldspar (K-feldspar and albite) and chlorite mixtures at elevated temperatures and pore pressures typifying geothermal reservoirs.

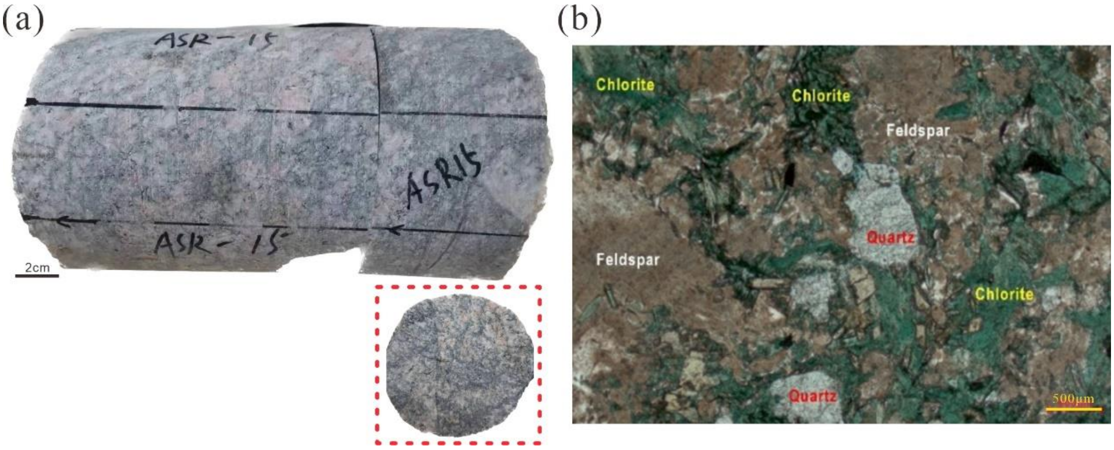

Figure 1. Photographs of (a) granite core recovered from ~4 km depth of the Matouying EGS reservoir in Tangshan, North China and (b) photomicrograph showing strong alteration of feldspar-chlorite.

2 Experimental Methods

We complete friction stability measurements on synthetic feldspar gouges representing chlorite alteration. Experiments are conducted under recreated hydrothermal conditions representative of deep geothermal systems to examine the influence of temperature, stress and pore pressures on friction and stability.

2.1 Gouge Preparation

The feldspar and chlorite minerals used to simulate fault gouges in our experiments were obtained commercially. The mineral compositions of the two mineral powders were analyzed by X-ray diffraction (XRD) and shown to be of >99 wt.% (feldspar) and 97 wt.% (chlorite) purity (Figure 2). The mineral composition of feldspar is 53 % K-feldspar and 47 % albite. To simulate fault gouge, both mineral powders were crushed and sieved to pass through a #200-mesh sieve. Median particle sizes of the feldspar (18.7 μm) and chlorite (66.9 μm) (Figure 3) are defined by laser classifier. Mixed gouges were then prepared from the feldspar and chlorite minerals in the same proportions by weight.

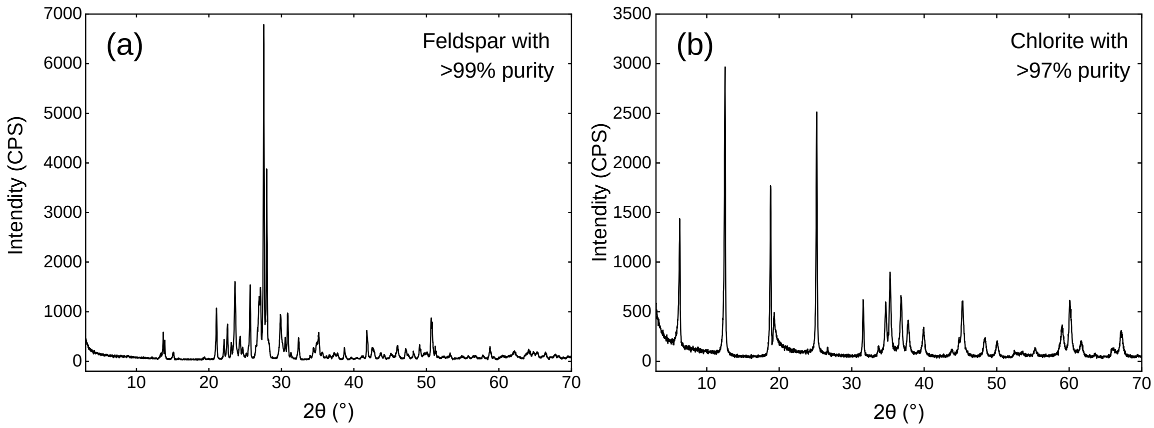

Figure 2. XRD results of feldspar and chlorite mineral powders used in the simulated fault gouges for the experiments. (a) feldspar purity at >99% and (b) chlorite purity at >97%.

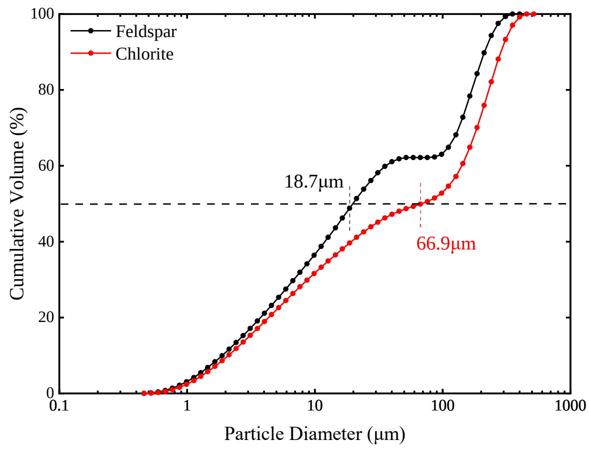

Figure 3. Particle size distributions of feldspar and chlorite gouges for the friction-stability experiments. The median particle sizes of the feldspar and chlorite gouges are 18.7 μm and 66.9 μm, respectively.

2.2 Apparatus and Experimental Procedure

Shear experiments were performed using an argon gas-confined triaxial testing apparatus (Figure 4) located at the Institute of Geology, China Earthquake Administration, Beijing, China (He et al., 2006, 2013). An electro-hydraulic servocontrol system drives the axial displacement in this apparatus that can apply a confining pressure up to 420 MPa, a temperature up to 600 °C, a fluid pressure up to 200 MPa, and an axial displacement rate down to 10^{-2} μm/s. We conducted shear experiments at temperature (T=180 °C) and pressure (P_c=95 MPa, P_f=35 MPa) conditions relevant to the depth of fluid injection for the 3.7 km Gonghe geothermal reservoir. We add deionized water to the mineral powders and bring them to chemical equilibrium by stirring for ~10 min. A 1-mm-thick layer of fault gouge was sandwiched between gabbro driving blocks 20 mm in diameter and 40 mm in height. The sawcut surface of the driving blocks is inclined at 35° to the loading axis. Two interconnected 2-mm-microboreholes in the upper driving block provide fluid access to the layer of fault gouge, and thus access to pore pressures. The assembled sample was jacketed in a 0.35-mm-thick annealed copper sleeve. Double O-rings seal both ends of the assembled sample to guard against incursion of the argon gas into the gouge layer. A thermocouple monitors the changes in temperature local to the fault gouge with the temperature maintained constant within ±1°C by an independent controller throughout each experiment. At the initiation of each experiment, we increase the confining pressure (argon gas), inject water to increase the pore pressure to 2/3 of the target pressure, heat to the target temperature and then fully pressurize to the desired value. Fluctuation in confining pressure and pore pressure were maintained constant within ±0.3 and ±0.1 MPa, respectively, through two servo-controlled intensifiers. All stress and displacement data were recorded at a sampling frequency of 1 Hz, except for a sampling frequency of 10 Hz at the maximum loading rate.

A total of 14 shear experiments were conducted at a constant confining pressure (P_c = 95 MPa), different pore pressures (P_f = 35, 50, 70 and 90 MPa) and different temperatures (T = 120, 180, 300, and 400°C) for monomineralic gouges (feldspar) and uniformly mixed feldspar: chlorite gouges (1:1). Experimental details are listed in Table 1. The results are representative of EGS development with the confining pressure P_c = 95 MPa and pore pressure P_f = 35 MPa corresponding to the lithostatic and hydrostatic pressures at ~3.7-km depth (assuming a rock density of 2,630 kg/m^3) in the EGS reservoir at Gonghe. In addition, the elevated pore pressures P_f = 50–90 MPa are consistent with fluid injection during reservoir stimulation. In the initial stage of the velocity stepping experiments, the gouge was sheared at a constant axial loading velocity of 0.5 μm/s until steady state friction was achieved. Then, the axial loading velocity was stepped between 5, 0.5 and 0.05 μm/s, corresponding to shear velocities of 6.1, 0.61 and 0.061 μm/s, to explore the frictional properties of the feldspar and mixed feldspar-chlorite gouges.

2.3 Data Analysis

The raw data of the shear experiments are corrected for the decrease in gouge contact area with shearing and the shear resistance from the copper jacket. The corrected data were then processed to obtain the corrected shear (τ) and normal stresses (σ_n). Frictional strength of the simulated fault gouge is defined by the frictional coefficient μ as

$$\mu = \frac{\tau}{\sigma_{neff}} = \frac{\tau}{(\sigma_n - P_f)} \quad (1)$$

where the σ_{neff} is the effective normal stress and P_f is the pore pressure.

The velocity dependence parameter *(a−b)* was estimated based on rate- and

-state-friction (RSF) theory (Dieterich, 1978; Ruina, 1983; Scholz, 1998). In the framework of RSF friction, the frictional coefficient μ is expressed as

$$\mu = \mu^{*} + aln\left(\frac{V}{V^{*}}\right) + bln\left(\frac{V^{*}\theta}{D_c}\right) \tag{2}$$

$$\frac{d\theta}{dt} = 1 - \frac{V\theta}{D_c} \tag{3}$$

where μ^* is the friction coefficient at the reference shear velocity V^*, a is the friction parameters reflecting the direct effect, b is the evolutionary effects of the shear velocity transition, with Dc denoting the critical slip distance over which frictional strength evolves to a new steady state. Equation (3) is the common evolution equation for the state variable θ, namely, the slowness law.

At a steady state friction, the state variable θ does not change with time t and thus $d\theta/dt=0$. Then, combining Equations (2) and (3), yields the frictional stability parameter *(a–b)* as

$$a - b = \frac{\mu - \mu^{*}}{\ln(V/V^{*})} \tag{4}$$

Positive values of *(a−b)* indicate that frictional coefficient increases with increasing velocity, namely, velocity strengthening behavior. Fault gouges with positive *(a−b)* promote inherently stable sliding and inhibit seismic rupture. Conversely, negative values of *(a−b)* indicate velocity weakening behavior and may host unstable fault slip if the fault system stiffness falls below the critical stiffness. Velocity-weakening behavior offers the potential for stick-slip and may result in earthquake nucleation (Marone, 1998; Scholz, 1998). The values of (*a–b)* under stable sliding can be recovered directly from the friction- displacement curves. Conversely, the values of (*a–b)* for quasi-static oscillations or stick-slip may be obtained from data fitting (described in detail in He et al., 2013), as completed here.

The potential for induced earthquakes requires that velocity- weakening conditions and a fault stiffness below the critical stiffness (K_{cr}) are both met. Fault instability results when (*a*–*b*) <0 and the loading stiffness K is smaller than the critical stiffness K_{cr}, that is, $K \leq K_{cr}$ (Gu et al., 1984). The critical stiffness of the fault (Ruina, 1983; He et al., 2013) is defined as

$$K_{cr} = \frac{-(a-b)\cdot\sigma_{neff}}{D_c} \tag{5}$$

where D_c is the characteristic slip distance and σ_{neff} is the effective normal stress. Due to the necessary condition of velocity weakening for the unstable sliding of faults, (*a*–*b*) is a topical parameter in shear experiments. Thus, we use the values of (*a*–*b*) as indices to explore the sliding behavior of faults in our study.

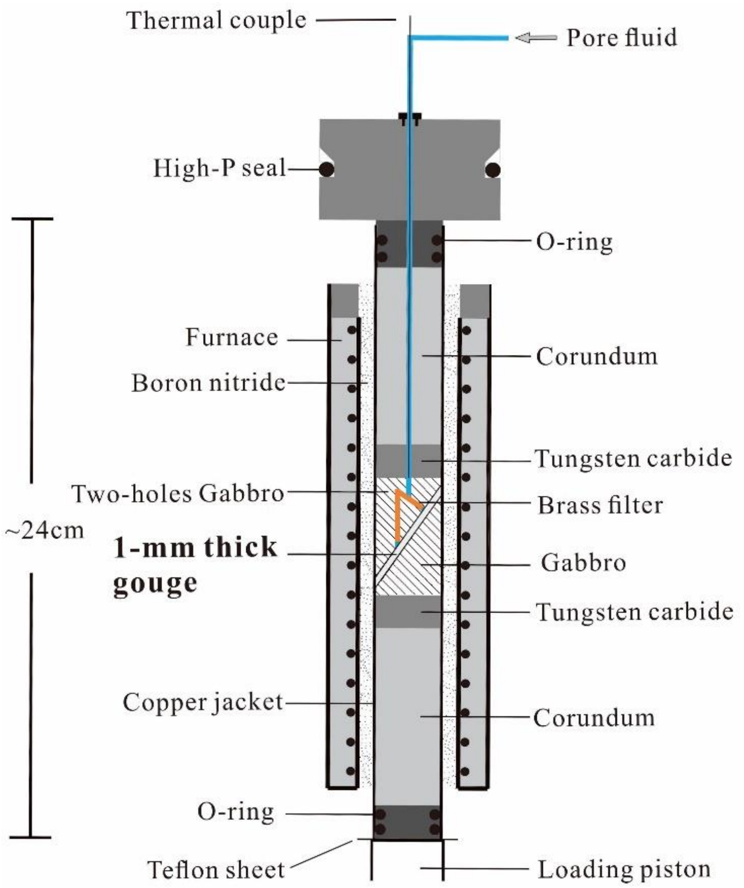

Figure 4. Schematic of the high-temperature and -pressure triaxial test apparatus. Both ends of the copper jacket are sealed with O-rings to prevent argon gas penetrating into the fault gouge sample. A high-pressure seal on the upper piston was used to prevent the leakage of the argon gas and retain the seal on the entire assembly.

2.4 Microstructural Methods

Post-shear, the corundum and tungsten carbide blocks were carefully removed with the gouge-filled gabbro driving blocks retained in the copper jacket. The samples were then placed into rubber molds-impregnated with epoxy resin in a vacuum chamber then cured in an oven at 65°C for ∼24 h until the epoxy had completely hardened. Thin sections were then prepared by slicing the hardened samples along shear and across the thin axis. All thin sections were polished and coated with carbon. With the microstructure observed using scanning electron microscopy (SEM).

Table 1. *Experimental matrix and key data*

Testing ID	Gouge	T (°C)	P_c (MPa)	P_f (MPa)	σ_{neff} (MPa)	l_{final} (mm)
Data set 1: Pure gouge at constant P_c=95 MPa						
CK-08	Fsp	120	95	35	118	3.49
CK-07	Fsp	180	95	35	117	3.71
CK-12	Fsp	180	95	50	89	4.04
CK-14	Fsp	180	95	70	52	3.53
CK-10	Fsp	180	95	90	13	3.20
CK-06	Fsp	300	95	35	120	3.32
CK-05	Fsp	400	95	35	120	3.64
Data set 2: Mixed gouges at constant P_c=95 MPa						
CK-09	50% Fsp+50% Chl	120	95	35	95	3.83
CK-01	50% Fsp+50% Chl	180	95	35	96	2.28
CK-11	50% Fsp+50% Chl	180	95	50	74	3.58
CK-13	50% Fsp+50% Chl	180	95	70	43	3.14
CK-02	50% Fsp+50% Chl	180	95	90	10	3.36
CK-04	50% Fsp+50% Chl	300	95	35	95	2.93
CK-03	50%Fsp+50% Chl	400	95	35	105	2.86

Note. Fsp=Feldspar, Chl=Chlorite, $P_{c=}$ confining pressure, P_f = pore fluid pressure, σ_{neff}= effective normal stress, T = temperature, l_{final} = final shearing displacement.

3 Results

We report experiments on both pure-feldspar and felspar-chlorite altered gouges to examine the impact of alteration of friction and frictional stability, and link response to microstructural observations.

3.1 Feldspar Gouge

The friction-displacement curves for the feldspar and mixed gouges initially exhibit a linear increase in friction (shear stress to normal stress ratio) with displacement followed by inelastic yield point then steady state friction at a shearing displacement of ~1.83 mm. This is in turn followed by slight strain hardening response until the final shear displacements of 3–4 mm (Table 1 and Figure S1 in Supporting Information). The simulated feldspar gouge shows stable sliding at T=120°C and P_f=35 MPa (Figure S1a in Supporting Information), while stick-slips were observed at a shear velocity of 0.061 μm/s at T = 180°C (Figure S1b in Supporting Information). As shown in Figure 4, the feldspar gouge exhibits a stable sliding at T>180 °C. A small oscillation lasting for ~0.1 mm of displacement occurs when the axial shear rate is switched to 5 μm/s at T=300 °C (Figure S1f in Supporting Information). The friction-displacement curves of the feldspar fault gouge show stable sliding and a strong dependence of friction coefficient on velocity (Figure S1g in Supporting Information). We measured the steady-state-friction coefficient at a shear displacement of ∼1.83 mm for each experiment. Our results show that the friction coefficient of feldspar gouge is ~ 0.71 over the range of experimental temperature (120–400°C), with no significant change with increasing temperature (Figure 5a). In contrast, the coefficients of friction μ for the simulated feldspar gouge at varied pore pressure are in the range ~ 0.70–0.87 and increase with pore pressure (Figure 5b).

Frictional stabilities (*a*–*b*) for the simulated feldspar gouge were obtained over the range of experimental temperature and pore pressure conditions (Table 2). A transition from velocity strengthening behavior (*a*–*b* =0.00016 to 0.00163) to velocity weakening behavior (*a*–*b* =-0.00098) can be identified at T=120–180 °C and P_f=35 MPa. This is then followed by a transition to velocity strengthening at T =300 °C (*a*–*b* =0.00108) and finally to velocity weakening at T = 400 °C (*a*–*b* =0.00101). This indicates that, temperature has a significant impact on stability of the feldspar gouge (Figure S2c in Supporting Information). At T=180 °C and P_f=35–90 MPa, the feldspar gouge exhibits velocity weakening behavior (*a*–*b* =-0.00098 to -0.00013). The velocity-weakening behavior of feldspar gouge decreases with increasing pore pressure at $P_f \geq 35$ MPa (Table 2 and Figure 5d). Moreover, the effective normal stress also significantly affects the velocity dependence of frictional stability. A higher effective normal stress returns a higher absolute value of *(a-b)* that increase nearly linearly with increasing effective normal stresses at T=180 °C (Figure 5e). In summary, higher effective normal stresses promote velocity-weakening behavior at constant temperature. In addition, we analyzed the variation of friction stability with shear velocity- the feldspar gouge exhibits a velocity-weakening behavior (*a*–*b*= -0.00270 to -0.00090) at lower shear velocities in the range of the experimental temperature (T=180–400 °C) and pressures (Figure 5a-b).

3.2 Mixed Feldspar-Chlorite Gouges

We evaluate the competing influences of feldspar and the alteration mineral chlorite on the frictional stability of the gouge. The shear experiments were conducted on the feldspar/chlorite mixed gouges at constant confining pressure P_c = 95 MPa, pore pressure P_f = 35–90 MPa, and temperature T = 120–400 °C. After ~1.83 mm of shear displacement, the friction- displacement curves exhibit a slight strain strengthening and stable sliding to a final shear displacement of 3–4 mm (Figure S2 in Supporting Information). The mixed gouges slide stably over the range of experimental temperature T = 120–300 °C (Figure S2a, S2b and S2f in Supporting Information). At T = 400 °C and for an axial loading rate V=0.5 μm/s, small oscillation in friction result, lasting ~0.2 mm, followed by stable sliding (Figure S2g in Supporting Information). The method for determining the frictional coefficient of the mixed gouges is identical to that for the feldspar gouge. The results show that the mean frictional coefficient for the mixed gouges is ~ 0.55, with the coefficient of friction μ at T = 400 °C deviating significantly from that at $T \leq 300$ °C (Figure 5a). The frictional strength increases with increasing pore pressure and the friction coefficient is less than that for the feldspar gouge over the range of experimental pore pressures (Figure 5b).

Trends in frictional stability *(a-b)* with applied temperature and pore pressure for the feldspar-chlorite mixed gouges are illustrated in Figure 5 and Table 2. This sample exhibits a transition from velocity weakening at T = 120°C and P_f=35 MPa (a-b =-0.00176) to slight velocity strengthening at $T \geqslant$ 180°C (a–b =0.00263 to 0.00443). Frictional stability *(a-b)* increases with increasing temperature when the axial displacement rates were stepped between 0.5 and 0.05 μm/s. Moreover, the value of *(a-b)* shows a variety of trends as the axial displacement rates were stepped between 0.5 and 5 μm/s (Figure 6). We compared velocity- dependent coefficient of friction for both the feldspar and mixed gouges, with the mixed gouges stronger than the feldspar at T > 120 °C (Figure 5c). The friction and stability of mixed gouges vary little with porosity at T=180℃ and P_f = 35–50 MPa - however, *(a-b)* values increase with increasing pore pressure at $P_f \geq$ 50 MPa. The frictional properties of the uniformly mixed gouges are significantly different from those of feldspar alone and change the trend as a function of pore pressure (Figure 5d). The velocity dependence parameter *(a-b)* of the mixed gouges first decreases and then increases with an increase in effective normal stress, with74 MPa as the transition stress (Figure 5e). The values of *(a-b)* decreases with increasing effective normal stress (σ_{neff}) at T = 180°C and σ_{neff}< 74 MPa. This can be interpreted as the lower-bound effective stress promoting velocity-strengthening behavior of the mixed fault gouge at constant temperature. Moreover, the sliding rate influences the frictional stability of the mixed gouges. The mixed feldspar-chlorite gouges exhibit velocity-strengthening behavior within the range of experimental temperature and pressures, and *(a-b)* reduces with an increase in shearing velocity (Figure 6c-d).

Table 2. *Results of Shear Experiments*

Test ID	μ_{ss}	a–b values at (μm/s)			
		6.1–0.61	0.61–0.061	0.061–0.61	0.61–6.1
CK-08	0.6998	0.00137±0.00046	0.00034±0.00016	0.00078	0.00163
CK-07	0.698	-0.00059±0.0003	-0.00145±0.00077	-0.00285	0.00099
CK-12	0.71	0.00051±0.00082	-0.0009±0.00014	-0.00264±0.00015	0.00016
CK-14	0.7451	0.00085±0.00039	-0.00095±0.00007	-0.00234±0.00057	0.0007
CK-10	0.8696	0.00045±0.00003	0.00165±0.00013	-0.00247±0.00021	-0.00016
CK-06	0.7161	0.00395	-0.00136	0.00022	0.00309
CK-05	0.7132	-0.00155±0.0005	-0.00112±0.00005	-0.0027	0.00134
CK-09	0.5291	0.00075±0.0007	-0.00336±0.00101	-0.0002±0.00063	-0.00242
CK-01	0.5352	0.00062	0.00391	0.00337	-
CK-11	0.5616	-0.00108±0.00241	0.00132±0.00059	0.00332±0.00084	-0.00016
CK-13	0.5909	0.00187±0.00105	0.00493±0.00021	0.00456±0.00061	0.0019
CK-02	0.6961	0.00385±0.00273	0.00531±0.0017	0.00407±0.00209	0.00397
CK-04	0.5264	0.00465±0.00043	0.00478	0.00434	0.00394
CK-03	0.6094	0.00311±0.0002	0.00565	0.00391	-0.00043

Note. The *(a–b)* values are the average values from the same velocity steps in each test with the error calculated from the standard deviation. Values of *(a–b)* at each shear velocity are also shown in Table S1 in the Supporting Information S1. The first velocity step (0.61–6.1 μm/s) was excluded in the calculation. μ_{ss} is the coefficient of friction determined at ~1.83 mm shear displacement.

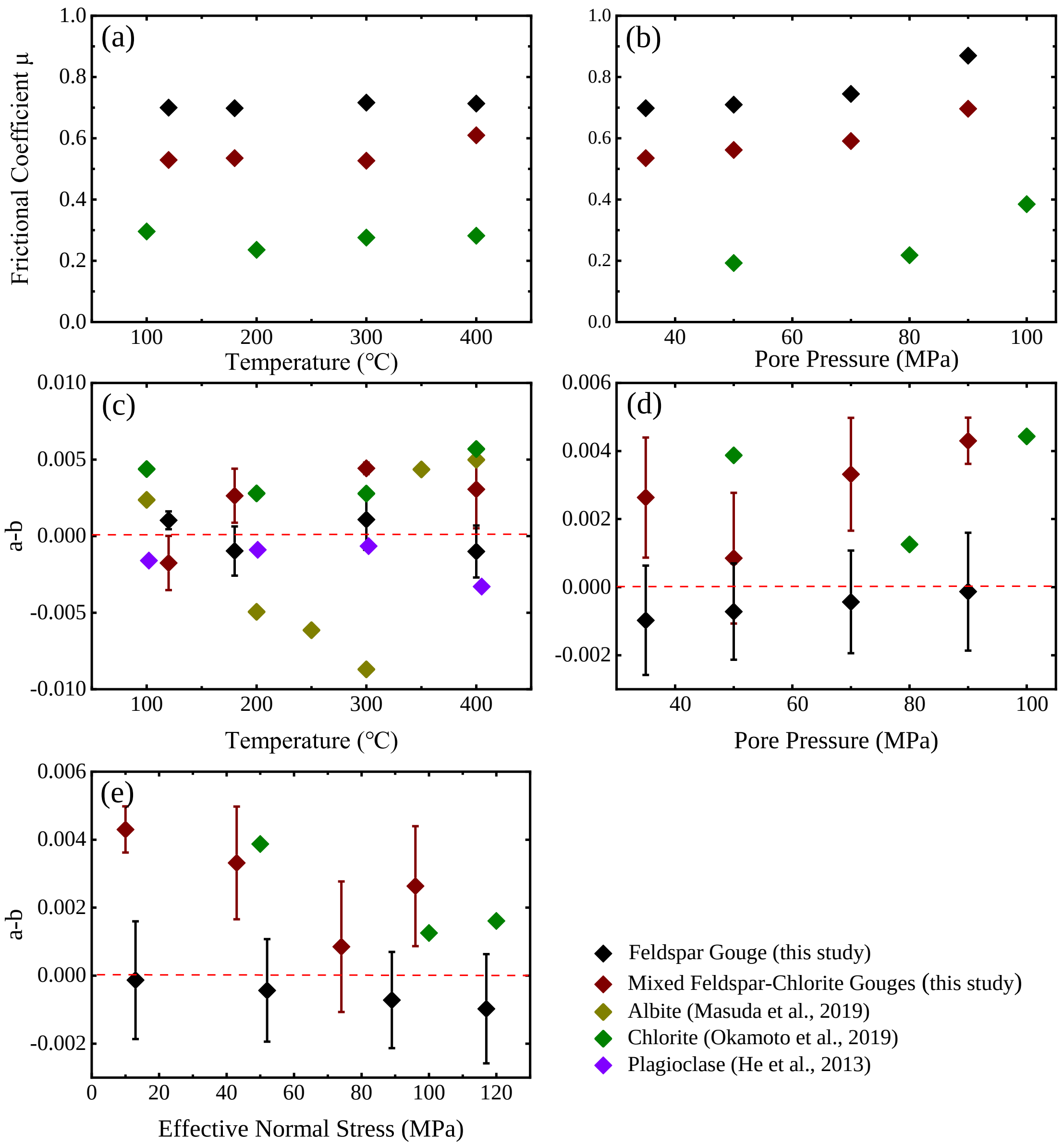

Figure 5. Coefficient of friction μ and frictional stability *(a–b)* for feldspar and feldspar-chlorite mixed gouges at varied conditions. (a) Values of μ versus temperature of pure feldspar gouge and mixtures at P_c = 95 MPa and P_f = 35 MPa. (b) Relationship between friction coefficient and pore pressure of pure gouge and mixtures at P_c = 95 MPa and T=180 ℃. (c) *(a-b)* as a function of temperatures for pure feldspar gouge and mixtures at P_c = 95 MPa and P_f = 35 MPa. The gray-green, green, and purple diamonds represent the results from Masuda et al. (2019), Okamoto et al. (2019) and He et al. (2013), respectively. (d) *(a–b)* as a function of pore pressure of pure gouge and mixtures at P_c = 95 MPa and T=180℃. (e) *(a–b)* as a function of effective normal stress of pure gouge and mixtures at P_c = 95 MPa and T=180℃.

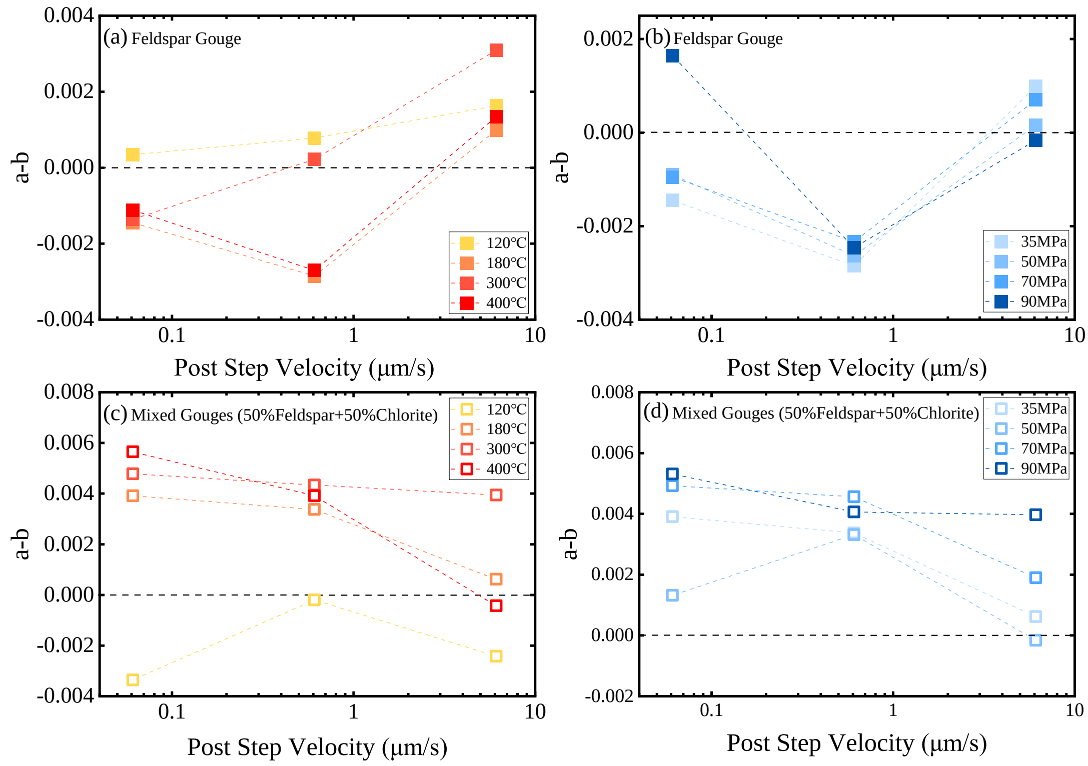

Figure 6. Frictional stability *(a-b)* for the feldspar and feldspar/chlorite mixed gouges at various post step velocities.

3.3 Microstructural Observations

Following the method described in Section 2.4, we performed microstructural observations on the deformed samples using scanning electron microscopy (SEM), with the methods of Logan et al. (1992) adopted to define the resulting fabric. Among, the post-experiment samples, disassembly destroyed the feldspar samples at P_f = 50 and 70 MPa and the mixed gouges at P_f = 70 MPa and T = 300°C. The fabrics of the gouge samples differ characteristically for the various gouge frictional responses (velocity-strengthening / velocity-weakening). Among them, grain size reduction appears to control the velocity-weakening behavior, and instability (Zhang et al., 2016; Casas et al., 2023). The microstructures of the deformed gouges are illustrated in Figures 9–10. At P_f=35 MPa and T=120–400°C, R_1 angle shears commonly develop in the feldspar gouge (Figure 7). The fault gouge exhibits velocity-weakening behavior with a narrow-localized shear zone with significant local grain crushing at T=180°C. Cracks tortuous penetrate throughout the fault zone (Figure 7b), although the number density of R_1 shear diminish with increasing temperature. At T=300–400°C, there are few R_1 fractures and local shear zones are inconspicuous that penetrate the fault zone in the gouge layer. When the temperature is increased to 400°C, the fault gouge exhibits a velocity weakening response and the extent of shear crack deflection is significantly higher than at 180 °C (Figure 7e). The number of R_1 shears in the feldspar gouge decreases with increasing pore pressure at T=180°C and P_f=35–90 MPa. At P_f= 90 MPa, uniformly shears evolve with pervasive particle crushing (<50 μm) for the deformed feldspar gouges (Figure 9), although no obvious

R_1 shear zone penetrates the fault gouge layer (Figure 7c). In addition, the gouge particles are sheared and uniformly crushed, with particle sizes ranging from a few micrometers to tens of micrometers at high pore pressure (P_f=90 MPa), i.e., at low effective stresses.

The chlorite particles are more fully comminuted than the feldspar particles in the mixed gouge (Figure S3 in Supporting Information). The number of R_1 shears in the mixed gouges increases with temperature at P_f=35 MPa and T=120–400°C (Figure 8), and the fault exhibits velocity-weakening behavior at T=120°C. At T=180–400°C, the gouge layer exhibits multiple cross-distributed groups of R_1 shears. The number of R_1 shear decreases with increasing pore pressure and a few parallel R_1 shears develop in the fault zone at T = 180 °C and P_f = 50 MPa (Figure 8c). However, the particles in the mixed fault gouge are sheared and crushed, with particle sizes ranging from few micrometers to nearly a hundred micrometers at P_f =90 MPa (Figure 8d).

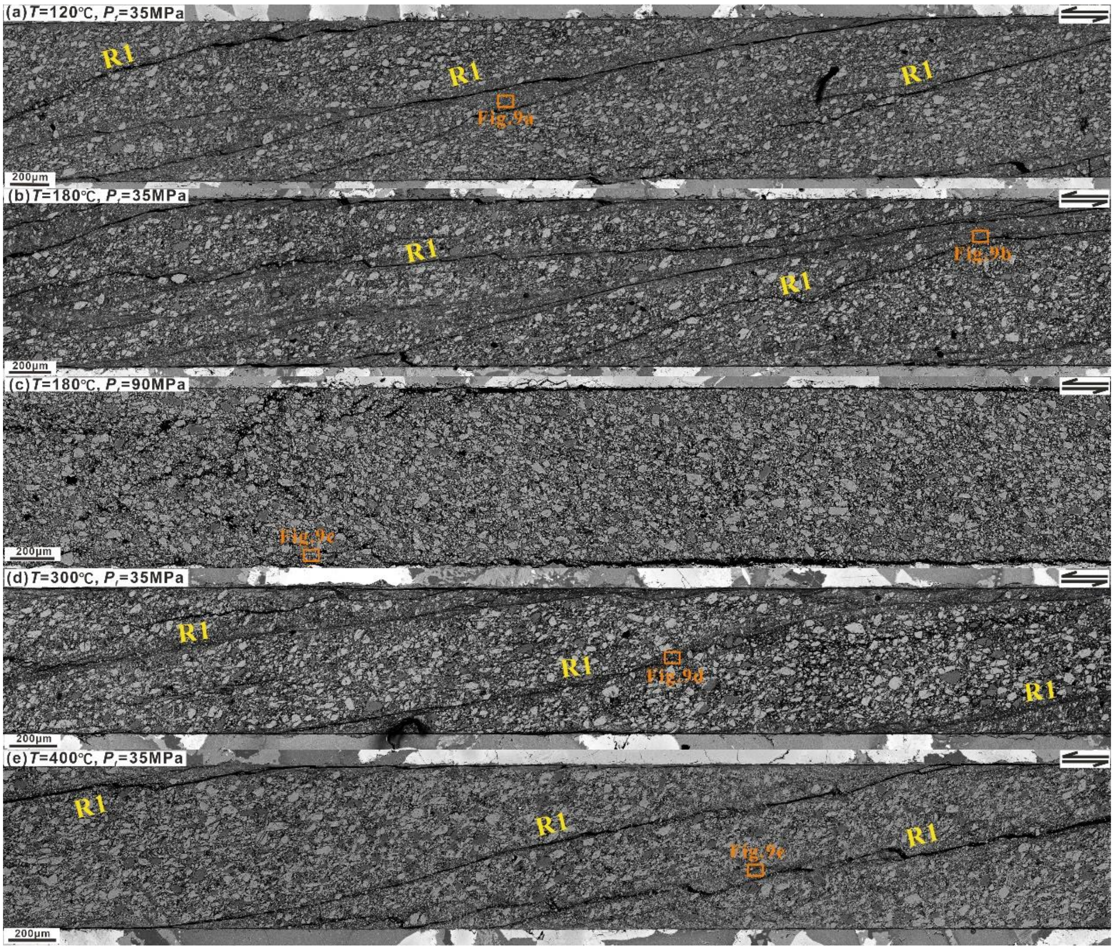

Figure 7. Microstructure (backscattered images) of the deformed feldspar gouge post-experiment. Refer to Logan et al. (1992) for relevant terms used to describe microscopic features. We observed local shear zones (LSZ) and R_1 shear (Riedel shear) in partial samples.

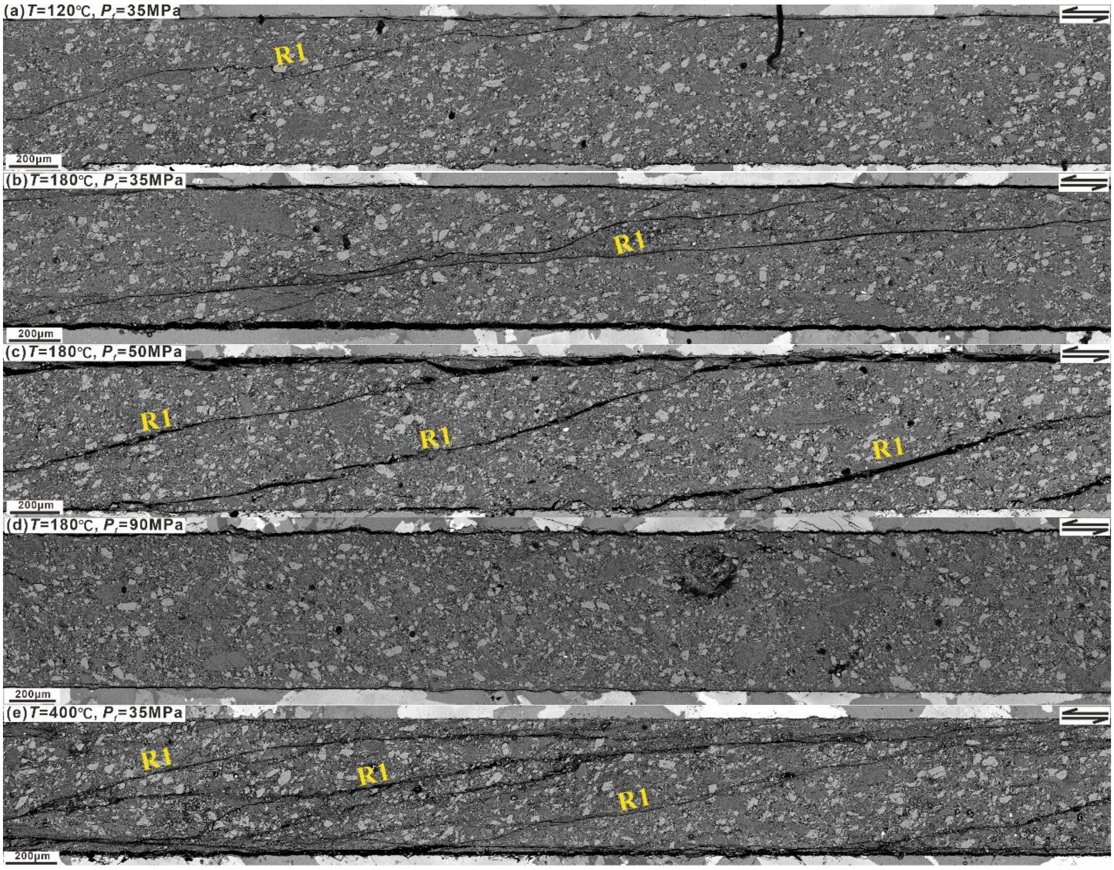

Figure 8. Microstructure (backscattered images) of the deformed feldspar/chlorite mixed gouges post-experiment. Refer to Logan et al. (1992) for relevant terms used to describe microscopic features. Experimental conditions: (a) T=120 ℃, P_f=35 MPa, (b) T=180 ℃, P_f=35 MPa, (c) T=180 ℃, P_f=50 MPa, (d) T=180 ℃, P_f=90 MPa, (e) T=400 ℃, P_f=35 MPa

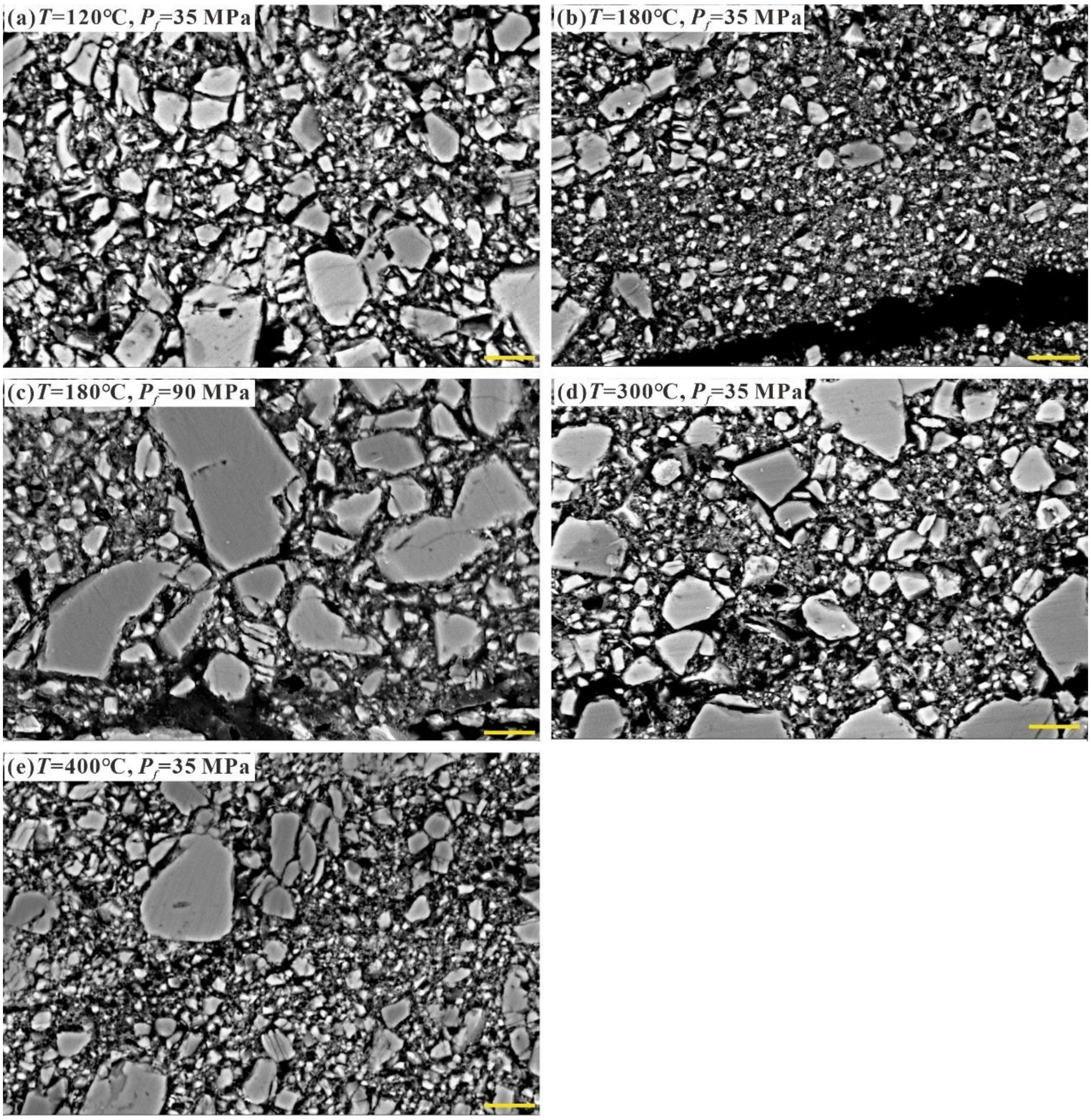

Figure 9. Particle fragmentation characteristics near the shear zone in the feldspar gouge after shearing. Among them, (b), (c) and (e) exhibit unstable sliding in velocity weakening. Scale bar: 5 μm.

4 Discussion

We explore impacts and mechanisms of temperature and pore pressure on both pure-feldspar (Section 4.1) and mixed feldspar-chlorite gouges (Section 4.2) in controlling friction and frictional stability. We use these observations and projected mechanisms to define implications for injection-induced seismicity (Section 4.3) in such common feldspar-chlorite altered systems.

4.1 Feldspar Stability Dependence on Temperature and Pore Pressure

The magnitudes of temperature and pore pressure are both important factors influencing fault instability (Blanpied et al., 1995). There is no significant variation in the frictional strength of the feldspar gouge with increasing temperature in our experiments. The average value of frictional coefficient for the feldspar gouge is ~0.7, consistent with previous experimental studies (Masuda, 2019, 2020; He et al, 2013). At P_f=35 MPa and T=120–400 °C, the feldspar gouge exhibits an evolving velocity dependence- velocity-strengthening behavior at T=120 °C and 300 °C and conversely velocity-weakening behavior at T=180 °C and 400 °C (Figure 5c). We also observe the apparent localized shear zones at this transition. The grain sizes in the localized shear zones significantly decreases increasing in the surface areas of the gouge and promoting unstable sliding (Bedford & Faulkner, 2021). Moreover, the feldspar gouge also shows a different transition in velocity dependence with the shear velocity stepping. For axial loading rates switched between 0.5 μm/s and 0.05 μm/s, the frictional stability coefficients *(a–b)* of the gouge decrease with increasing temperature. The transition from velocity-strengthening to velocity-weakening in our shear experiments can commonly be explained by a microphysical model (Niemeijer & Spiers, 2007; den Hartog et al., 2012; Chen et al., 2015, 2016). The model assumes that the strength and velocity dependence of the gouge is regulated by the competition between an expansion velocity (due to intergranular particle flow) and a compaction velocity (due to thermally activated pressure solution). The velocity of pressure solution increases with an increase in temperature and the gouge is further compacted. When the compaction velocity of the gouge particles is approximately equal to the expansion velocity then velocity-weakening behavior results (Verberne et al., 2020; Chen et al., 2020). Although we did not observe remarkable features indicating pressure solution for our range of experimental temperatures, previous experimental studies have indeed indicated the presence of intergranular pressure solution in feldspar minerals at higher temperatures (He et al., 2013). Thus, our experimental results are consistent with such a model. Our experimental results show a velocity-strengthening behavior at T= 300°C which transforms to velocity weakening at T=400°C (Figure 5c), which is inconsistent with the above microphysical model. However, we note that our experimental conditions of T = 300 and 400 °C and P_f = 35 MPa approach those for supercritical water (T = 374 °C, P_f = 22.1 MPa; Maxim et al., 2021). Solubility of solutes and reaction rates in the supercritical state are significantly elevated (Weingärtner & Franck, 2005) and thus may impact intergranular pressure solution. Therefore, when the temperature exceeds the critical point between 300-400°C, the density of the water will change drastically (Sakuma & Ichiki, 2016) and may promote an elevated rate of pressure solution of feldspar in the range of 300°C to 400°C. This, combined with the microstructural observation that localized shear zones disappear at T=300 °C – suggests that feldspar undergoes a decomposition reaction and produces other alteration minerals such as chlorite at T=300 °C, and thus changes the chemical composition of the gouge (Yuguchi et al., 2021), which then affects the frictional behavior. However, this conjecture requires further analysis of the post-experimental sample composition.

Our experimental results show that the effect of pore pressure on the frictional stability of gouge exhibits specific trends at constant temperature (Figure 5d). The frictional strength of feldspar gouge increases with increasing pore pressure, showing velocity weakening behavior, but the velocity dependence coefficient (*a*–*b*) increases linearly with increasing pore pressure. Previous systematic studies of quartz solubility have shown that quartz solubility increases with increasing pore pressure at the identical temperature (Anderson & Burnham, 1965), and feldspar follows a similar pro-grade solubility trend. Thus, the rate of feldspar pressure solution increases with increasing pore pressure. This is consistent with the above microphysical model. That is, that the pressure solution of feldspar becomes more vigorous and effective as a dissolution-diffusion process with an increase in pore pressure at the same experimental conditions- thus increasing the intergranular compaction velocity and decreasing porosity. As the intergranular contact area decreases, the gouge frictional strength increases and the value of (*a*–*b*) also gradually increases. Few distinct R_1 shear zones are observed in the microstructures of our experiments at P_f= 90 MPa, rather, exhibiting uniform shear fragmentation. The deformation of the gouge is dominated by rolling at high pore pressure and low effective stresses, and thus brittle rupture processes may be masked by the disappearance of localized shear zones in the gouge. Thus, the feldspar gouge exhibits velocity-weakening behavior at high pore pressure, but with no obvious local shear zones observed in the microstructure.

4.2 Influence of Mineral Composition on Fault Friction

Fault may transition from strengthen to weaken over long fluid-injection timescales at elevated temperatures, due to secondary mineral precipitation of hydrothermal alteration (Jeppson et al., 2023). Chlorite, as a low frictional strength altered mineral (Ikari et al., 2009; Okamoto et al., 2020; An et al., 2021) reduces the overall frictional strength of the mixed gouges. The frictional coefficients of the feldspar-chlorite mixed gouge were significantly lower than those of the feldspar gouge over the range of experimental temperatures. There is no clear evolution of the frictional coefficient of the mixed gouge with increasing temperature at $T \leqslant 300$ °C (Figure 5a). Chlorite has a low coefficient of friction (μ = 0.25–0.30) over our range of experimental temperature (⩽400 °C) and does not change significantly with temperature (Okamoto et al., 2019, 2020). Therefore, we speculate that the sudden increase in the frictional coefficient of the mixed gouges from 0.55 to 0.61 at *T*= 400°C is due to the impact of K-feldspar chloritization (Yuguchi et al., 2021). The frictional strengths of the feldspar-chlorite mixed gouges increase with increasing pore pressure. Moreover, the frictional strength of the feldspar gouge varies consistently for both contents at different temperatures and pore pressures. Our results show that the presence of chlorite in the gouge overall reduces the strength but does not change the trend in frictional strength. The velocity dependence of the mixed gouges over the range of experimental temperatures reveals that the mixed gouges exhibit both velocity-weakening and velocity-strengthening behavior, and that the velocity dependence parameter *(a-b)* increases with increasing temperature.

Our results indicate that the effect of different pore pressures on the frictional properties of feldspar-chlorite mixed gouges is similar to that of temperature. The frictional strength of the mixed gouges is significantly lower than that of the feldspar gouge and increases with increasing pore pressure. There is a consistent trend of frictional strength of gouges with pore pressure for the two feldspar contents (1:0 and

1:1). The feldspar-chlorite mixed gouges show velocity-strengthening behavior that increases with increasing pore pressure. The variation of *(a-b)* values with pore pressure is nearly linear at $P_f \geq$ 50 MPa (Figure 5d). The frictional stability of the mixed gouges is significantly enhanced compared to the feldspar gouge due to the presence of chlorite. Combining with the observations of microstructural characteristics of the deformed samples, we find that the number of R_1 shear decreases with increasing pore pressure. Moreover, compared with the frictional stability of chlorite (Okamoto et al., 2019), albite (Masuda et al., 2019) and plagioclase (He et al., 2013) from previous experiments, the presence of feldspar minerals reduces the frictional stability of the mixed gouges (Figure 5c-e). The stability of the feldspar gouge increases with an increase in pore pressure.

4.3 Implication for Injection-Induced Seismicity

These results have important implications in understanding the mitigation of induced seismicity at different temperatures and pore pressures in granitic EGS (enhanced geothermal system) reservoirs. EGS requires the injection of cold fluids (typically water) into the subsurface which typically results in a significant increase in pore pressure and a reduction in effective stress. Fluid transport relies on a connected network of natural and artificial fractures. Unexpectedly, large amounts of fluid may access undetected critical stress faults (Grigoli et al., 2018), with alteration minerals conditioning the strength and stability of such faults (An et al., 2021, 2022). In high-temperature fractured reservoirs, the enhanced artificial circulation fluid volume will further accelerate the consumption of feldspar and the occurrence of chlorite. This effect will lead to a decrease in the strength of exposed faults, as confirmed by laboratory friction experiments and microstructural observations (Jeppson et al., 2023). Our experimental results show that the feldspar gouge presents velocity-weakening behavior at $T \geqslant 180$ °C. This indicates that feldspar-rich faults may undergo unstable sliding as the depth of the modified reservoir increases, but the feldspar/chlorite mixed gouges may promote stable sliding of faults, which implies that feldspar chloritization in EGS reservoirs of granite rock is a process with dynamic competitive effects. Furthermore, our experimental results suggest that the process of feldspar to chlorite transformation has an influential role in the unstable sliding of faults. The results of our shear experiments demonstrate that temperature alone may not be the main determinative factor contributing to seismicity in granitic EGS reservoirs and highlights the importance of pore pressures. Meanwhile, high temperature may promote the fluid–assisted processes and modulate the local stresses in reservoirs (den Hartog et al., 2012; Martínez- Garzón et al., 2014; Chen et al., 2015; Westaway & Burnside, 2019). Hence, the combined effect of temperature and pore pressure may be important in triggering seismicity in feldspar-rich EGS reservoirs.

In addition, other compounding factors cannot be neglected in the triggering of earthquakes in EGS reservoirs, such as in situ driving slip rates. Our experiments show that the velocity dependence of feldspar gouge weakens with decreasing shearing rate. Feldspar gouge exhibits velocity weakening behavior at axial shear velocities of ~0.5 μm/s and ~0.05 μm/s (Figure 6), which suggests that unstable sliding of the fault occurs at low rates of shear sliding and thus may induce seismicity. The natural driving slip rates of the faults are much lower than those utilized in the laboratory (Chen et al., 2015). Thus, lower tectonic driving velocities may further reduce frictional stability, that is, induce smaller and more negative values of (*a*–*b*) and then cause unstable sliding of the faults. Further experimental studies are needed to analyze the effects of different mineral contents and shear velocity on fault stability. Our results have implications for natural faults that may undergo feldspar-chlorite alteration processes and are present at elevated temperatures and pressures in the subsurface.

5 Conclusions

Based on the hydrothermal conditions at the depth of the granitic EGS reservoir, we conducted shear experiments to explore the frictional stability of simulated feldspar (K-feldspar and albite) gouge and feldspar/chlorite mixed gouge. Meanwhile, the effects of different temperatures and pore pressures on fault sliding were analyzed. The experimental results show that the frictional strength of chlorite-rich mixed gouges is lower than that of feldspar gouge. The microstructural observation reveals that the chlorite particles are more strongly sheared. Thus, the decrease in frictional strength with increasing chlorite content may be explained by this phenomenon. The velocity dependence enhances with increasing chlorite content, which suggests that the content of clay minerals in the gouge may be one of the controlling factors for the frictional behavior of the fault. Additionally, the velocity dependence of feldspar gouge enhances and the values of the velocity dependence coefficients (*a*–*b*) increase with increasing pore pressure under hydrothermal conditions. Combined with the analysis of the effects of temperature and pore pressure, we hypothesize that fluid injection operations within the depth range of the EGS modification may promote unstable sliding of potentially feldspar-rich faults, which suggests that feldspar-rich faults may be reactivated in granitic EGS reservoirs. Hence, the presence of feldspar chloritization sequences and the range of injection pressures needs to be considered in the development of EGS to minimize the risk of injection-induced seismicity.

Acknowledgments

The research was funded by National Natural Science Foundation of China (No. 42177175), Central Public-interest Scientific Institution Basal Research Fund (No. DZLXJK202204), and China Geological Survey (Nos. DD20190138, DD20221660). We thank Prof. Changrong He for useful discussions of the raw test data. We appreciate the assistance of Wenming Yao and Xi Ma in running the original experiments. DE gratefully acknowledges support from the G. Albert Shoemaker endowment.

Data Availability Statement

The experimental data presented in this study are available at https://doi.org/10.5061/dryad.4b8gthtkc

References

Anderson, G. M., & Burnham, C. W. (1965). The solubility of quartz in super-critical water. *American Journal of Science*, 263(6), 494–511. https://doi.org/10.2475/ajs.263.6.494.

Andrés, S., Santillán, D., Mosquera, J. C., & Cueto- Felgueroso, L. (2019). Delayed weakening and reactivation of rate- and- state faults driven by pressure changes due to fluid injection. *Journal of Geophysical Research: Solid Earth*, 124, 11,917–11,937. https://doi.org/10.1029/2019JB018109.

An, M., Zhang, F., Chen, Z., Elsworth, D., & Zhang, L. (2020). Temperature and fluid pressurization effects on frictional stability of shale faults reactivated by hydraulic fracturing in the Changning block, southwest China. *Journal of Geophysical Research: Solid Earth*, 125, e2020JB019584. https://doi.org/10.1029/2020JB019584.

An, M., Zhang, F., Min, K. B., Elsworth, D., Marone, C., & He, C. (2021). The potential for low‑grade metamorphism to facilitate fault instability in a geothermal reservoir. *Geophysical Research Letters*, 48(11). https://doi.org/10.1029/2021GL093552.

An, M., Zhang, F., Min, K.-B., Elsworth, D., He, C., & Zhao, L. (2022). Frictional stability of metamorphic epidote in granitoid faults under hydrothermal conditions and implications for injection-induced seismicity. *Journal of Geophysical Research: Solid Earth*, 127, e2021JB023136. https://doi.org/10.1029/2021JB023136.

Bao, X., & Eaton, D. W. (2016). Fault activation by hydraulic fracturing in western Canada. *Science*, 354(6318), 1406-1409. https://doi.org/10.1126/science.aag2583.

Bedford, J. D., & Faulkner, D. R. (2021). The role of grain size and effective normal stress on localization and the frictional stability of simulated quartz gouge. *Geophysical Research Letters*, 48, e2020GL092023. https://doi.org/10.1029/2020GL092023.

Brown, K. M., Kopf, A., Underwood, M. B., & Weinberger, J. L. (2003). Compositional and fluid pressure controls on the state of stress on the Nankai subduction thrust: A weak plate boundary. *Earth and Planetary Science Letters*, 214(3–4), 589–603. https://doi.org/10.1016/S0012-821X(03)00388-1.

Blanpied, M. L., Lockner, D. A., & Byerlee, J. D. (1991). Fault stability inferred from granite sliding experiments at hydrothermal conditions. *Geophysical Research Letters*, 18(4), 609–612. https://doi.org/10.1029/91GL00469.

Blanpied, M. L., Lockner, D. A., & Byerlee, J. D. (1995). Frictional slip of granite at hydrothermal conditions. *Journal of Geophysical Research: Solid Earth*, 100(B7), 13045–13064. https://doi.org/10.1029/95JB00862.

Casas, N., Mollon, G., & Daouadji, A. (2023). Influence of grain-scale properties on localization patterns and slip weakening within dense granular fault gouges. *Journal of Geophysical Research: Solid Earth*, 128, e2022JB025666. https://doi.org/10.1029/2022JB025666.

Chen, J., Verberne, B. A., & Spiers, C. J. (2015). Effects of healing on the seismogenic potential of carbonate fault rocks: Experiments on samples from the Longmen Shan Fault, Sichuan, China. *Journal of Geophysical Research: So* *lid Earth*, 120(8), 5479–5506. https://doi.org/10.1002/2015JB012051.

Chen, J., & Spiers, C. J. (2016). Rate and state frictional and healing behavior of carbonate fault gouge explained using microphysical model. *Journal of Geophysical Research: Solid Earth*, 121(12), 8642–8665.https://doi.org/10.1002/2016JB013470.

Chen, J., Verberne, B. A., & Niemeijer, A. R. (2020). Flow‐to‐friction transition in simulated calcite gouge: Experiments and microphysical modeling. *Journal of Geophysical Research: Solid Earth*, 125(11). https://doi.org/10.1029/2020JB019970.

den Hartog, S. A., Peach, C. J., de Winter, D. M., Spiers, C. J., & Shimamoto, T. (2012). Frictional properties of megathrust fault gouges at low sliding velocities: New data on effects o-f normal stress and temperature. *Journal of Structural Geology*, 38, 156–171. https://doi.org/10.1016/j.jsg.2011.12.001.

Dieterich, J. H. (1978). Preseismic fault slip and earthquake prediction. *Journal of Geophysical Research: Solid Earth*, 83(B8), 3940–3948. https://doi.org/10.1029/JB083iB08p03940.

Elders, W. A., Hoagland, J. R., Mcdowell, S. D., & Cobo, J. (1979). Hydrothermal mineral zones in the geothermal reservoir of Cerro Prieto. *Geothermics*, 8(3–4), 201–209. https://doi.org/10.1016/0375-6505(79)90042-7.

Ellsworth, W. L. (2013). Injection-induced earthquakes. *Science*, 341(6142), 1225942. https://doi.org/10.1126/science.1225942.

Er-yong Zhang; Dong-guang Wen; Gui-ling Wang et al. (2022). The first power generation test of hot dry rock resources exploration and production demonstration project in the Gonghe Basin, Qinghai Province, China. *China Geology*, Vol.5(3): 372–382. https://doi.org/10.31035/cg2022038.

Eyre, T. S., Eaton, D. W., Garagash, D. I., Zecevic, M., Venieri, M., Weir, R., & Lawton, D. C. (2019). The role of aseismic slip in hydraulic fracturing-induced seismicity. *Science Advances*, 5(8), 1–11. https://doi.org/10.1126/sciadv.aav7172.

Fagereng, Å., & Ikari, M. J. (2020). Low‐temperature frictional characteristics of chlorite‐epidote‐amphibole assemblages: Implications for strength and seismic style of retrograde fault zone-s. *Journal of Geophysical Research: Solid Earth*, 125(4), e2020JB019487. https://doi.org/10.1029/2020JB019487.

Faulkner, D. R., Sanchez-Roa, C., Boulton, C., & den Hartog, S. A. M. (2018). Pore fluid pressure development in compacting fault gouge in theory, experiments, and nature. *Journal of Geophysical Research: Solid Earth*, 123, 226–241. https://doi.org/10.1002/2017JB015130.

Fengshou Zhang，Mengke An，Lianyang Zhang，Yi Fang，Derek Elsworth. (2020). Effect of mineralogy on friction-dilation relationships for simulated faults: Implications for permeability evolution in caprock faults. *Geoscience Frontiers,* (11): 439–450. https://doi.org/10.1016/j.gsf.2019.05.014.

F. M. Chester; N. G. Higgs. (1992). Multimechanism Friction Constitutive Model for Ultrafine Quartz Gouge at Hypocentral Conditions. *Journal of Geophysical Research. Part B: Solid Earth*, 97: 1859–1870. https://doi.org/10.1029/91JB02349.

Grigoli, F., Cesca, S., Rinaldi, A. P., Manconi, A., López-Comino, J. A., Clinton, J. F., Wiemer, S. (2018). The November 2017 Mw5.5 Pohang earthquake: A possible case of induced seismicity in South Korea. *Science*, 360(6392), 1003–1006. https://doi.org/10.1126/science.aat2010.

Gu, J. C., Rice, J. R., Ruina, A. L., & Tse, S. T. (1984). Slip motion and stability of a single degree of freedom elastic system with rate and state dependent friction. *Journal of the Mechanics and Physics of Solids*, 32(3), 167–196. https://doi.org/10.1016/0022-5096(84)90007-3

He, C., Yao, W., Wang, Z., & Zhou, Y. (2006). Strength and stability of frictional sliding of gabbro gouge at elevated temperatures. *Tectonophysics*, 427(1–4), 217–229. https://doi.org/10.1016/j.tecto.2006.05.023.

He, C., Luo, L., Hao, Q. M., & Zhou, Y. (2013). Velocity‐weakening behavior of plagioclase and pyroxene gouges and stabilizing effect of small amounts of quartz under hydrothermal conditions. *Journal of Geophysical Research: Solid Earth*, 118(7), 3408–3430. https://doi.org/10.1002/jgrb.50280.

Hubbert, M. K., & Rubey, W. W. (1959). Role of fluid Pressure in mechanics of overthrust faulting. *Geological Society of America Bulletin*, 70(2), 115–166. https://doi.org/10.1130/0016-7606(1959)70[115:ROFPIM]2.0.CO;2.

Hunfeld, L. B., Niemeijer, A. R., & Spiers, C. J. (2017). Frictional properties of simulated fault gouges from the seismogenic Groningen gas field under in situ P–T -chemical conditions. *Journal of Geophysical Research: Solid Earth*, 122, 8969–8989. https://doi.org/10.1002/2017JB014876.

Ikari, M. J., Saffer, D. M., & Marone, C. (2009). Frictional and hydrologic pr operties of clay‐rich fault gouge. *Journal of Geophysical Research: Solid E arth*, 114(B5). https://doi.org/10.1029/2008JB006089.

Ikari, M. J., Marone, C., & Saffer, D. M. (2011). On the relation between fault strength and frictional stability. *Geology*, 39(1), 83–86. https://doi.org/10.1130/G31416.1.

Jeppson, T. N., Lockner, D. A., Beeler, N. M., & Moore, D. E. (2023). Time-dependent weakening of granite at hydrothermal conditions. *Geophysical Research Letters*, 50, e2023GL105517. https://doi.org/10.1029/2023GL105517

John D. Bedford, Daniel R. Faulkner & Nadia Lapusta. (2022). Fault rock heterogeneity can produce fault weakness and reduce fault stability. *Nature communications*, Vol.13(1): 326, https://doi.org/10.1038/s41467-022-27998-2.

Lockner, D. A., Summers, R., & Byerlee, J. D. (1986). Effects of temperature and sliding rate on frictional strength of granite. *Pure and Applied Geophysics*, 124(3), 445–469. https://doi.org/10.1007/BF00877211.

Logan, J. M., Dengo, C. A., Higgs, N. G., & Wang, Z. Z. (1992). Fabrics of experimental fault zones: Their development and relationship to mechanical behavior. In *International geophysics*, 51, 33–67. Academic Press. https://doi.org/10.1016/S0074-6142(08)62814-4.

Lucie Mathieu. (2016). Quantifying hydrothermal alteration with normative minerals and other chemical tools at the Beattie Syenite, Abitibi greenstone belt, Canada. *EOCHEMISTRY-EXPLORATION ENVIRONMENT ANALYSIS*, Vol.16: 233–244. https://doi.org/10.1144/geochem2016-410.

Majer, E. L., Baria, R., Stark, M., Oates, S., Bommer, J., Smith, B., & Asanuma, H. (2007). Induced seismicity associated with enhanced geothermal systems.

Geothermics, *36*(3), 185–222. https://doi.org/10.1016/j.geothermics.2007.03.003.

Marone, C. (1998). Laboratory-derived friction laws and their application to seismic faulting. Annual Review of Earth and Planetary Sciences, 26(1), 643–696. https://doi.org/10.1146/annurev.earth.26.1.643.

Martínez- Garzón, P., Kwiatek, G., Sone, H., Bohnhoff, M., Dresen, G., & Hartline, C. (2014). Spatiotemporal changes, faulting regimes, and source parameters of induced seismicity: A case study from the Geysers geothermal field. *Journal of Geophysical Research: Solid Earth*, 119, 8378–8396. https://doi.org/10.1002/2014JB011385.

Masuda, K.; Arai, T.; Takahashi, M. (2019) Effects of frictional properties of quartz and feldspar in the crust on the depth extent of the seismogenic zone. *Progress in Earth and Planetary Science*, 6(1): 1–8, https://doi.org/10.1186/s40645-019-0299-5.

Masuda, Koji. (2020). Frictional properties of anorthite (feldspar): implications for the lower boundary of the seismogenic zone. *Earth, Planets & Space*, Vol.72(1): 1–6, https://doi.org/10.1186/s40623-020-01271-6.

Maxim, F., Karalis, K., Boillat, P., Banuti, D. T., Marquez Damian, J. I., Niceno, B., & Ludwig, C. (2021). Thermodynamics and dynamics of supercritical water pseudo-boiling. *Advanced Science*, 8(3). https://doi.org/10.1002/advs.202002312.

Morrow, C. A., Moore, D. E., & Lockner, D. A. (2000). The effect of mineral bond strength and adsorbed water on fault gouge frictional strength. *Geophysical Research Letters*, 27(6), 815–818. https://doi.org/10.1029/1999GL008401.

Niemeijer, A. R., & Spiers, C. J. (2007). A microphysical model for strong velocity weakening in phyllosilicate-bearing fault gouges. *Journal of Geophysical Research*, 112, B10405. https://doi.org/10.1029/2007JB005008.

Okamoto, A. S., Verberne, B. A., Niemeijer, A. R., Takahashi, M., Shimizu, I., Ueda, T., & Spiers, C. J. (2019). Frictional properties of simulated chlorite gouge at hydrothermal conditions: Implications for subduction megathrusts. *Journal of Geophysical Research: Solid Earth*, 124(5), 4545–4565. https://doi.org/10.1029/2018JB017205.

Okamoto, A. S., Niemeijer, A. R., Takeshita, T., Verberne, B. A., & Spiers, C. J. (2020). Frictional properties of actinolite-chlorite gouge at hydrothermal conditions. *Tectonophysics*, 779, 228377. https://doi.org/10.1016/j.tecto.2020.228377.

Ruina, A. (1983). Slip instability and state variable friction laws. *Journal of Geophysical Research: Solid Earth*, 88(B12), 10359–10370. https://doi.org/10.1029/JB088iB12p10359.

Sakuma, H., & Ichiki, M. (2016). Density and isothermal compressibility of supercritical H2O–NaCl fluid: molecular dynamics study from 673 to 2000 K, 0.2 to 2 GP a, and 0 to 22 wt% NaCl concentrations. *Geofluids*, 16(1), 89–102. https://doi.org/10.1111/gfl.12138.

Schiffman, P., & Fridleifsson, G. O. (1991). The smectite-chlorite transition in drillhole NJ-15, Nesjavellir geothermal field, Iceland: XRD, BSE and electron microprobe investigations. *Journal of Metamorphic Geology*, 9(6), 679–696. https://doi.org/10.1111/j.1525-1314.1991.tb00558.x.

Scholz, C. (1998). Earthquakes and friction laws. *Nature*, 391, 37–42.

https://doi.org/10.1038/34097.
Scholz, C. (2019). The Mechanics of Earthquakes and Faulting (3rd ed.). Cambridge: Cambridge University Press. https://doi.org/10.1017/9781316681473.
Schultz, R., Skoumal, R. J., Brudzinski, M. R., Eaton, D., Baptie, B., &Ellsworth, W. (2020). Hydraulic fracturing-induced seismicity. *Reviews of Geophysics*, 58, e2019RG000695. https://doi.org/10.1029/2019RG000695.
Shimamoto, T., & Logan, J. M. (1981). Effects of simulated clay gouges on the sliding behavior of Tennessee sandstone. *Tectonophysics*, 75(3–4), 243–255. https://doi.org/10.1016/0040-1951(81)90276-6.
Yuguchi, T., Sasao, E., Ishibashi, M., & Nishiyama, T. (2015). Hydrothermal chloritization processes from biotite in the Toki granite, Central Japan: Temporal variations of the compositions of hydrothermal fluids associated with chloritization. *American Mineralogist*, 100(5–6), 1134–1152. http://dx.doi.org/10.2138/am-2015-5126.
Takashi Yuguchi, Takanobu Matsuki, Yuya Izumino, Eiji Sasao, Tadao Nishiya ma (2021), Mass transfer associated with chloritization in the hydrothermal a lteration process of granitic pluton. *American Mineralogist*; 106 (7): 1128–11 42. https://doi.org/10.2138/am-2020-7353.
Tembe, S., D. A. Lockner, and T.-F. Wong (2010), Effect of clay content and mineralogy on frictional sliding behavior of simulated gouges: Binary and ternary mixtures of quartz, illite, and montmorillonite, *Journal of Geophysical Research: Solid Earth*, 115, B03416, https://doi:10.1029/2009JB006383.
van der Elst, N. J., Savage, H. M., Keranen, K. M., & Abers, G. A. (2013). Enhanced remote earthquake triggering at fluid- injection sites in the midwestern United States. *Science*, 341(6142), 164–167. https://doi.org/10.1126/science.1238948.
Verberne, B. A., van den Ende, M. P., Chen, J., Niemeijer, A. R., & Spiers, C. J. (2020). The physics of fault friction: Insights from experiments on simulated gouges at low shearing velocities. *Solid Earth Discussions*, 2020, 1–37. https://doi.org/10.5194/se-11-2075-2020.
Weingärtner, H., & Franck, E. U. (2005). Supercritical water as a solvent. *Angewandte Chemie International Edition*, 44(18), 2672–2692. https://doi.org/10.1002/anie.200462468.
Westaway, R., & Burnside, N. M. (2019). Fault “corrosion” by fluid injection: A potential cause of the November 2017 Mw 5.5 Korean earthquake. *Geofluids*, 2019, 1–23. https://doi.org/10.1155/2019/1280721.
Zhang, F., Huang, R., An, M., Min, K. B., Elsworth, D., Hofmann, H., & Wa ng, X. (2022). Competing Controls of Effective Stress Variation and Chloritiz ation on Friction and Stability of Faults in Granite: Implications for Seismici ty Triggered by Fluid Injection. *Journal of Geophysical Research: Solid Eart h*, 127(8). https://doi.org/10.1029/2022JB024310.
Zhang, L., and C. He (2016), Frictional properties of phyllosilicate-rich mylonit e and conditions for the brittle-ductile transition, *J. Geophys. Res. Solid Eart h*, 121, 3017–3047. https://doi.org/10.1002/2015JB012489.
Zhen Lu, Changrong He. (2018). Friction of foliated fault gouge with a biotite

interlayer at hydrothermal conditions. *Tectonophysics*, 740, 72–92. https://doi.org/10.1016/j.tecto.2018.05.003.